



Cite this: *J. Mater. Chem. A*, 2015, 3, 19920

Received 18th June 2015  
Accepted 20th August 2015

DOI: 10.1039/c5ta04474j

www.rsc.org/MaterialsA

## Amorphous $\text{Na}_2\text{Si}_2\text{O}_5$ as a fast $\text{Na}^+$ conductor: an *ab initio* molecular dynamics simulation

Xueling Lei,<sup>ab</sup> Youngseok Jee<sup>b</sup> and Kevin Huang<sup>\*b</sup>

The present work uses the *ab initio* molecular dynamics (AIMD) methodology to simulate ionic transport in amorphous and crystalline  $\text{Na}_2\text{Si}_2\text{O}_5$  from 573 to 973 K. The results suggest that amorphous  $\text{Na}_2\text{Si}_2\text{O}_5$  is primarily a  $\text{Na}^+$  conductor with negligible  $\text{O}^{2-}$  and  $\text{Si}^{4+}$  contributions to ionic conduction, whereas crystalline  $\text{Na}_2\text{Si}_2\text{O}_5$  is virtually an electrical insulator. The favorable pathway for  $\text{Na}^+$  transport in amorphous  $\text{Na}_2\text{Si}_2\text{O}_5$  is along the two-dimensional channels formed by the  $\text{SiO}_4$  tetrahedral layers. The disrupted Na–O coulombic attraction by the long-range disorder in amorphous  $\text{Na}_2\text{Si}_2\text{O}_5$  contributes to the enhanced  $\text{Na}^+$  conduction.

### I. Introduction

The pursuit of high-conductivity solid electrolyte materials has long been of interest to solid-state chemists/electrochemists because of the significance it can bring to advance the development of high-power, high-capacity and efficient electrochemical cells such as fuel cells and batteries for a variety of energy applications.<sup>1–3</sup> Recently, a new family of oxides bearing a generic formula of  $\text{Sr}_{1-x}\text{A}_x\text{SiO}_{3-0.5x}$  ( $\text{A} = \text{Na}, \text{K}$ ) has been reported and immediately garnered much attention due to its high ionic conductivity, *e.g.*  $0.01 \text{ S cm}^{-1}$  at  $500^\circ\text{C}$ .<sup>4–7</sup> The report quickly drew criticisms from groups that conducted follow up research.<sup>8–13</sup> These studies presented compelling evidence that the material was virtually a two-phase mixture, for example, consisting of a  $\text{SrSiO}_3$  phase and an amorphous  $\text{Na}_2\text{Si}_2\text{O}_5$  phase for the  $\text{Sr}_{1-x}\text{Na}_x\text{SiO}_{3-0.5x}$  system.<sup>9–13</sup> The  $\text{SrSiO}_3$  phase was an electrical insulator while the amorphous  $\text{Na}_2\text{Si}_2\text{O}_5$  phase was a good ionic conductor. The high conductivity observed in  $\text{Sr}_{1-x}\text{Na}_x\text{SiO}_{3-0.5x}$  essentially stemmed from the amorphous  $\text{Na}_2\text{Si}_2\text{O}_5$  phase. However, the nature of ionic conduction in amorphous  $\text{Na}_2\text{Si}_2\text{O}_5$ , *e.g.*  $\text{Na}^+$  vs.  $\text{O}^{2-}$ , has remained ambiguous until now.

Early MD simulations of ionic diffusion in glassy  $\text{Na}_2\text{Si}_2\text{O}_5$  have focused mainly in the higher temperature range.<sup>14–16</sup> For example, Smith *et al.* simulated the ionic transport for sodium disilicate glass in a temperature range of 1000–2000 K in one study<sup>14</sup> and for alkali-metal disilicate glasses at 1400 K in another study.<sup>16</sup> No work has been reported so far on solid-state amorphous  $\text{Na}_2\text{Si}_2\text{O}_5$  in a lower temperature range such as below 1000 K. In the present study, we aim to elucidate the ionic conduction mechanisms in amorphous  $\text{Na}_2\text{Si}_2\text{O}_5$  from a

computational perspective, *i.e.* applying the *ab initio* molecular dynamics (AIMD) methodology to simulate ionic transport in solid-state amorphous  $\text{Na}_2\text{Si}_2\text{O}_5$  in a temperature range of 573–973 K, a preferred operating temperature range for reduced-temperature solid oxide fuel cells (SOFCs). The work is of great importance not only to the understanding of ionic conduction mechanisms of solid-state  $\text{Sr}_{1-x}\text{A}_x\text{SiO}_{3-0.5x}$ , but also to the identification of new solid-state ionic conductors in the future.

### II. The simulation method

The first-principles calculations in this study were performed using the projector augmented wave (PAW) method<sup>17,18</sup> included in a commercial VASP code.<sup>19,20</sup> The  $\text{Na } 2p^6 3s^1$ ,  $\text{O } 2s^2 2p^4$ , and  $\text{Si } 3s^2 3p^2$  electrons were considered as valence electrons. The general gradient approximation (GGA) parameterized by Perdew–Burke–Ernzerhof (PBE) was used for the exchange–correlation terms,<sup>21</sup> and wave functions were expanded by plane waves with a cut-off energy of 500 eV. The atomic positions were optimized until residual ionic forces became less than  $0.02 \text{ eV } \text{\AA}^{-1}$ .

For the *ab initio* molecular dynamics (AIMD) simulations of ionic transport, the canonical ensemble (NVT) was employed. A Verlet algorithm was integrated with Newton's equations of motion at a time step of 2 fs for a total simulation time of 40 ps, *i.e.*, 20 000 steps. The frequency of the temperature oscillations was controlled by the Nosé mass during the simulations. A supercell of  $1 \times 2 \times 2$  unit cells (144 atoms) was used with a *k*-point sampling at the *T*-point.

To create an amorphous structure, the supercell was first melted by virtually heating it to 5000 K within the NVT ensemble. Then, a melt configuration was randomly chosen to test the optimal lattice constant while considering the change in system volume induced by the phase transition. Finally, the

<sup>a</sup>Department of Physics, Jiangxi Normal University, Nanchang, Jiangxi 330022, China

<sup>b</sup>Department of Mechanical Engineering, University of South Carolina, Columbia, SC 29208, USA. E-mail: huang46@cec.sc.edu

melt configuration was subjected to a cooling process at a rate of  $2.67 \times 10^{13} \text{ K s}^{-1}$  to obtain an amorphous structure.

For comparison, Na-ion transport in crystalline  $\text{Na}_2\text{Si}_2\text{O}_5$  was also simulated, in which a supercell of  $1 \times 2 \times 2$  (144 atoms) with a  $2 \times 2 \times 1$   $k$ -point grid sampling was used together with the nudged elastic band (NEB) to seek for the saddle points and minimum energy pathways.<sup>22,23</sup>

### III. Results and discussion

#### 3.1. $\text{Na}^+$ diffusion in amorphous $\text{Na}_2\text{Si}_2\text{O}_5$

**3.1.1 Structure and electronic properties of a  $\text{Na}_2\text{Si}_2\text{O}_5$  crystal.**  $\text{Na}_2\text{Si}_2\text{O}_5$  has a triclinic structure (SG:  $P1$ ), the unit cell of which is depicted in Fig. 1(a) as  $\text{SiO}_4$  layers with  $\text{Na}^+$  residing in between the corner-shared  $\text{SiO}_4$  layers for charge compensation. From the calculated density of states (DOSs), Fig. 1(b), the band gap of the crystalline  $\text{Na}_2\text{Si}_2\text{O}_5$  is 4.22 eV, which essentially indicates that it is an electrical insulator. The calculated lattice constants and structural parameters listed in Table 1 agree well with the experimental data,<sup>24</sup> validating the computational method and parameters used.

**3.1.2 Testing lattice constants of amorphous  $\text{Na}_2\text{Si}_2\text{O}_5$ .** To perform a rational AIMD simulation under the required constant volume condition in the VASP code, the system volume change induced by the phase-transition needs to be determined so that an appropriate volume can be applied to the calculation. To do so, the optimal lattice constants of the amorphous  $\text{Na}_2\text{Si}_2\text{O}_5$  structure need to be obtained first. As described in Section II, a melt configuration was randomly chosen and relaxed for 40 ps at each volume. Fig. 2 shows the average free energy vs. lattice constant scale factor. It is evident that the influence of volume on the free energy is relatively small. The best lattice constant scale factor was found to be 1.015, implying a 4.5% volume expansion after melting. In the following AIMD

simulations, the lattice parameters of all the structures were multiplied by 1.015, aiming to more accurately calculate the potential energy and free energy.

**3.1.3 Structure and radial distribution function ( $g(r)$ ).** The AIMD simulations within the NVT ensemble were conducted in a temperature range of 573–973 K. The amorphous structures were obtained by the methods described in Section II. As an example, Fig. 3(a) and (b) compare the amorphous structure simulated at 973 K with the crystalline structure. To extract the structural information, the present study calculated the radial distribution function (RDF),  $g(r)$ , for the total and partial properties. Fig. 3(c) and (d) show the total  $g(r)$  as a function of radius ( $r$ ) for crystalline and amorphous  $\text{Na}_2\text{Si}_2\text{O}_5$ , respectively. For the crystalline  $\text{Na}_2\text{Si}_2\text{O}_5$ , crystallographic ordering is clearly seen at both the long- and short-range scale, whereas only a short-range ordering is observed for amorphous  $\text{Na}_2\text{Si}_2\text{O}_5$ . In specific, there are two sharp peaks at a radius of 1.65 and 2.65 Å for amorphous  $\text{Na}_2\text{Si}_2\text{O}_5$ , corresponding to the nearest Si–O and O–O separations, respectively, and a shoulder at 2.35 Å associated with the nearest Na–O separation. These RDF distributions are in good agreement with those obtained from neutron diffraction on the same  $\text{Na}_2\text{Si}_2\text{O}_5$  glass;<sup>25</sup> the latter study revealed two sharp peaks at a radius of 1.7 and 2.6 Å, and a broad peak at a radius of 2.4 Å associated with the nearest Na–O separation.

The partial RDF for amorphous  $\text{Na}_2\text{Si}_2\text{O}_5$  simulated at 973 K is further plotted in Fig. 4; the results for other temperatures are similar. From the peak positions in a partial RDF, the peaks that appeared in the total RDF shown in Fig. 3(d) can be further interpreted. For example, the strong first peak at a radius of 1.65

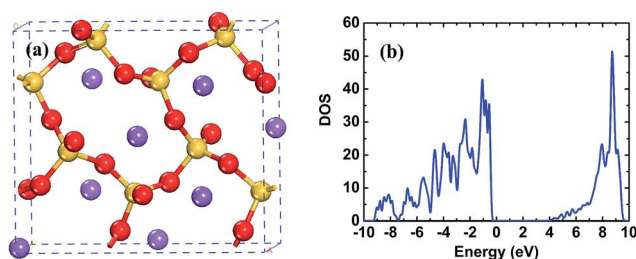


Fig. 1 (a) The structure of the  $\text{Na}_2\text{Si}_2\text{O}_5$  unit cell; (b) and corresponding density of states DOSs. The red, golden, and purple balls represent the O, Si, and Na ions, respectively.

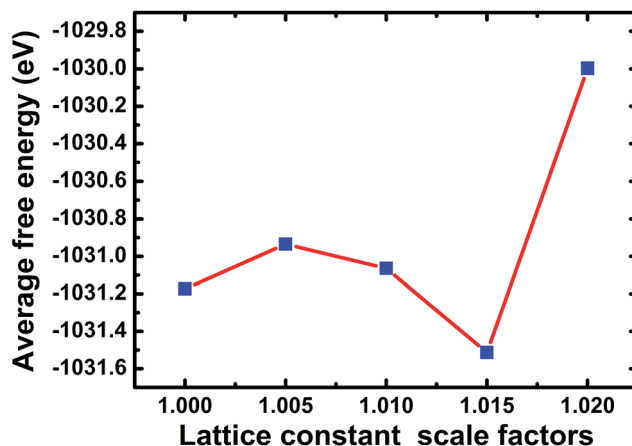


Fig. 2 The average free energy versus the lattice constant scale factors.

**Table 1** Calculated lattice constants, structural parameters and corresponding experimental values of crystalline  $\text{Na}_2\text{Si}_2\text{O}_5$  sodium disilicate considered in this work. The units of length and angle are angstrom (Å) and degree (°), respectively.  $\text{O}_{\text{br}}$  and  $\text{O}_{\text{nbr}}$  denote the bridging and nonbridging O atoms, respectively

	<i>A</i>	<i>b</i>	<i>C</i>	$\alpha = \beta = \gamma$	Si– $\text{O}_{\text{br}}$	Si– $\text{O}_{\text{nbr}}$	Si–O–Si
Calculated (this work)	9.539	5.656	8.468	90	1.658–1.674	1.591–1.595	125.9–129.0
Experimental	9.441	5.580	8.356	90	1.633–1.656	1.571–1.580	127.0–129.3

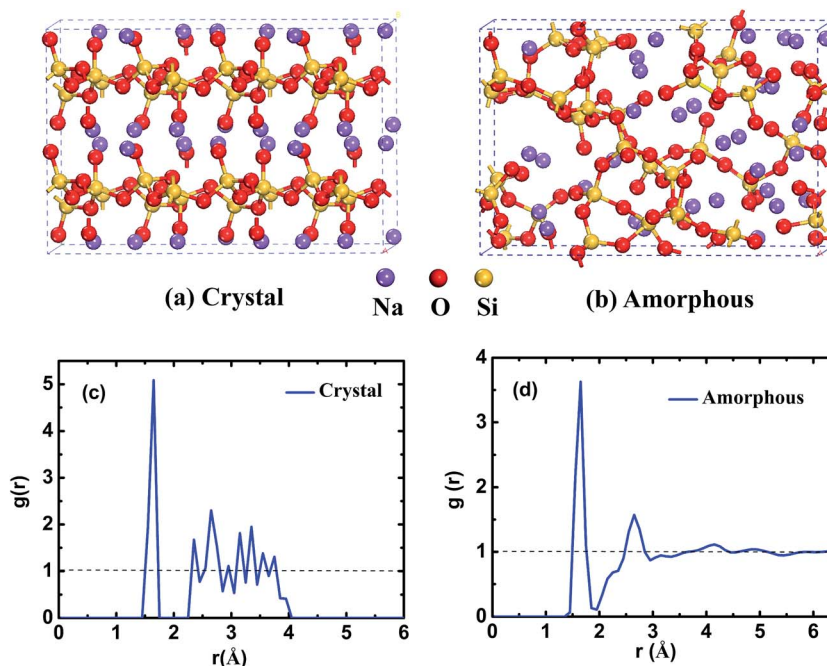


Fig. 3 The structures of (a) crystalline and (b) amorphous  $\text{Na}_2\text{Si}_2\text{O}_5$ , and total radial distribution function of (c) crystalline and (d) amorphous  $\text{Na}_2\text{Si}_2\text{O}_5$  simulated at 973 K.

Å in the partial Si–O RDF is responsible for the first peak in the total RDF. Integration of the partial Si–O RDF indicates 3.92 O atoms surrounding each Si atom, indicating  $\text{SiO}_4$  tetrahedral units are present in amorphous  $\text{Na}_2\text{Si}_2\text{O}_5$ . The first peak at a radius of 2.35 Å in the partial Na–O RDF is weak in the simulated total RDF. The strong first peak in the partial O–O RDF agrees well with the prominent peak in the total RDF at a radius of 2.65 Å, which reflects the O–O separation in a  $\text{SiO}_4$  tetrahedron. The second strong peak in the partial O–O RDF is at a radius of 4.95 Å. A simple estimate from the atomic structure suggests that this peak is associated with the O–O separation from one tetrahedron to the other. The first peaks in the partial Si–Si and Na–Si RDF at radii of 3.05 and 3.15 Å, respectively, appear to be responsible for the weak features in the same region of the total RDF. Finally, it is noted that the first peak in the partial Na–Na RDF at a radius of 3.25 Å is almost invisible in the total RDF, implying a fast  $\text{Na}^+$  transport.

**3.1.4 Mean-squared displacement, diffusion coefficient, and conductivity.** From a statistical physics perspective, the random diffusion of an ionic species in a material can be described by the mean square displacement (MSD). It is well known that the plots of MSDs for all ions feature plateaus independent of time for a poor conductor, whereas they exhibit a monotonic increase with time for a good conductor. The MSD of ions in a simulation can be computed by:

$$\begin{aligned} \text{MSD} &= \langle \delta r^2 \rangle = \left\langle [r_m(t+t_0) - r_m(t_0)]^2 \right\rangle \\ &= \frac{1}{N} \sum_m [r_m(t+t_0) - r_m(t_0)]^2 \end{aligned} \quad (1)$$

where  $N$  is the total number of ions, and  $r_m(t+t_0)$  and  $r_m(t_0)$  are the displacements of the  $m^{\text{th}}$  ion at  $t+t_0$  and  $t_0$  time,

respectively. The chevrons represent ensemble average. In the present work, a total of three MD simulations were performed for the same structure at each temperature, aiming to obtain an averaged MSD for accuracy. Fig. 5 shows the average MSD calculated for  $\text{Na}^+$ ,  $\text{O}^{2-}$ , and  $\text{Si}^{4+}$  in amorphous  $\text{Na}_2\text{Si}_2\text{O}_5$  from 573 to 973 K. Evidently, the MSD of  $\text{Na}^+$  increases linearly with time, indicating a fast  $\text{Na}^+$  transport. In contrast, the MSDs of  $\text{O}^{2-}$  and  $\text{Si}^{4+}$  are almost parallel to the time axis, implying immobile  $\text{O}^{2-}$  and  $\text{Si}^{4+}$ . The distinct feature in Fig. 5 strongly suggests that  $\text{Na}^+$  is the predominant charge carrier in amorphous  $\text{Na}_2\text{Si}_2\text{O}_5$ .

The average self-diffusion coefficient ( $D$ ) of ions can be determined from the slope of the average MSD plots:

$$D = \lim_{t \rightarrow \infty} \frac{\langle \delta r^2 \rangle}{6t} \quad (2)$$

However, one should keep in mind that  $D$  herein is not a chemical diffusion coefficient used in Fick's equation describing diffusion flux of species under a chemical concentration gradient. Instead, it is a self-diffusion coefficient describing the ability to diffuse under no concentration gradient. The correlation between the self-diffusion coefficient  $D$  and direct current ionic conductivity  $\sigma$  is given by the Nernst-Einstein relationship:

$$\sigma_{\text{dc}} = \frac{N_{\text{ion}} q^2 D}{H_{\text{R}} k_{\text{B}} T} \quad (3)$$

here  $N_{\text{ion}}$  and  $q$  are the number density and charge of the mobile ion, respectively;  $k_{\text{B}}$  is Boltzmann's constant;  $T$  is the absolute temperature;  $H_{\text{R}}$  is the Haven ratio between the tracer diffusivity  $D^*$  and charge diffusivity  $D_{\sigma}$ :  $H_{\text{R}} = D^*/D_{\sigma}$ , describing the

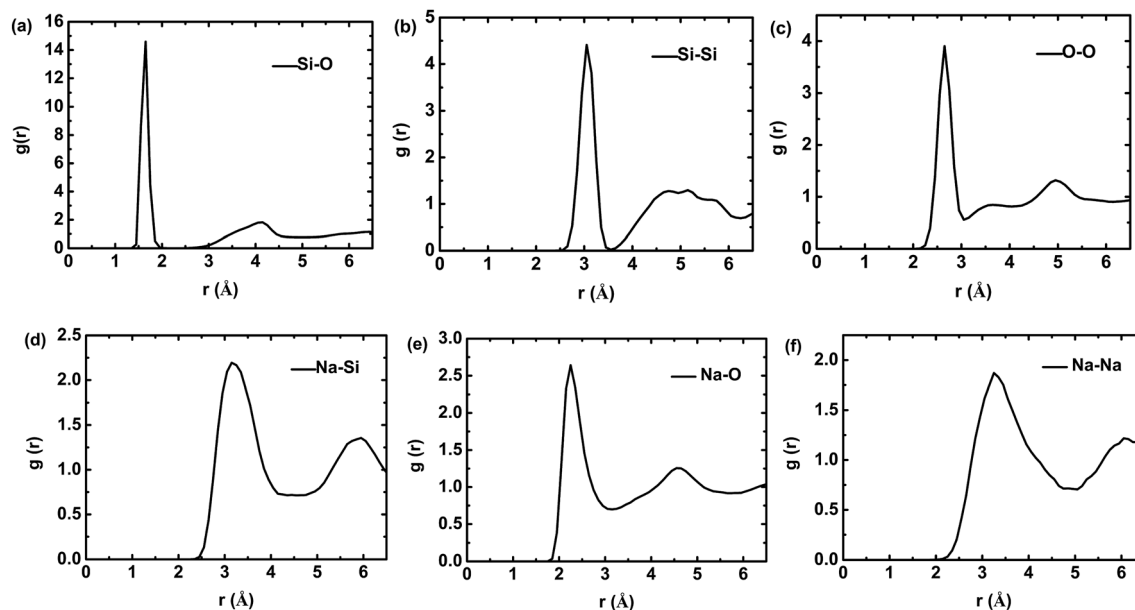


Fig. 4 Partial radial pair distribution function for amorphous  $\text{Na}_2\text{Si}_2\text{O}_5$  simulated at 973 K.

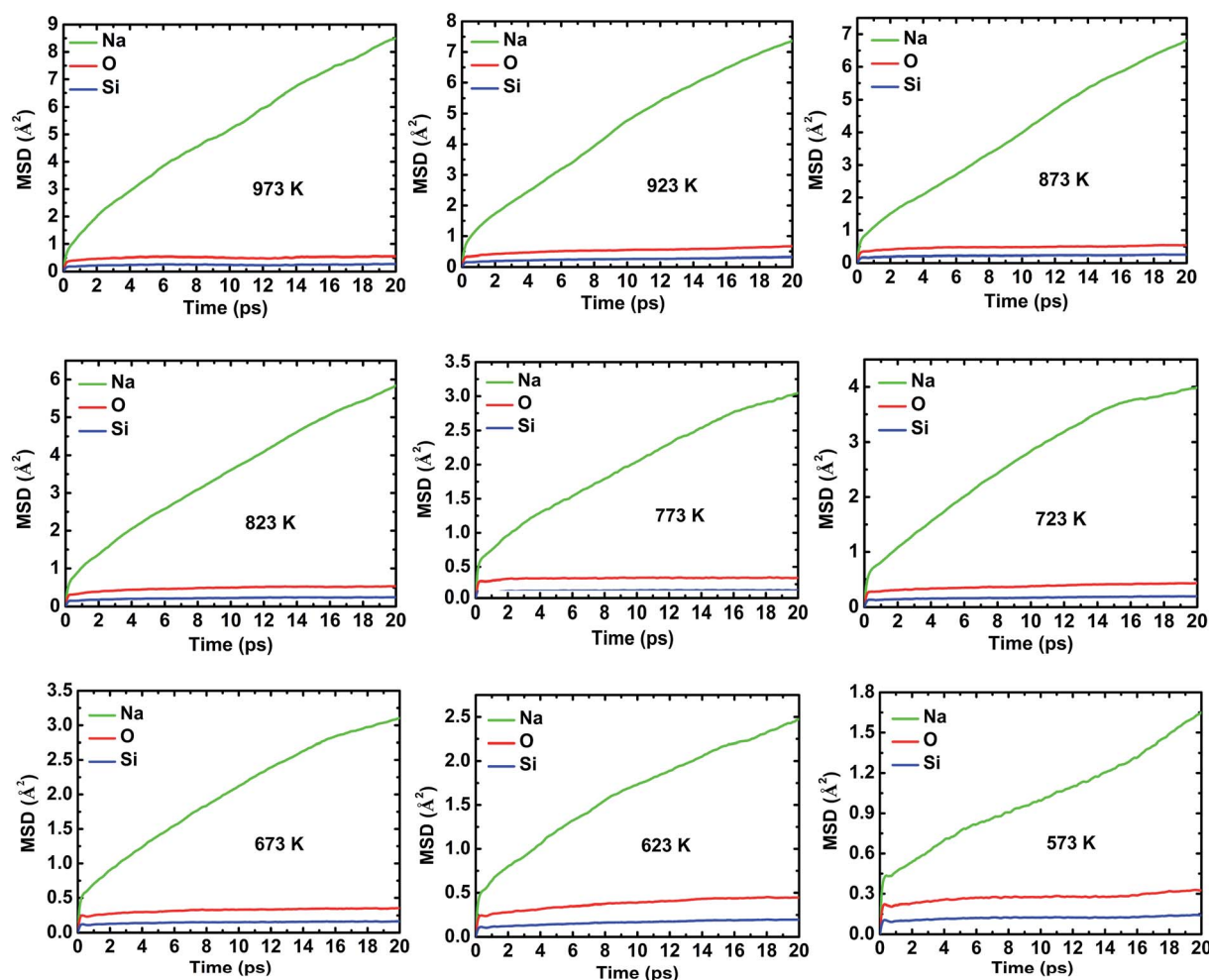
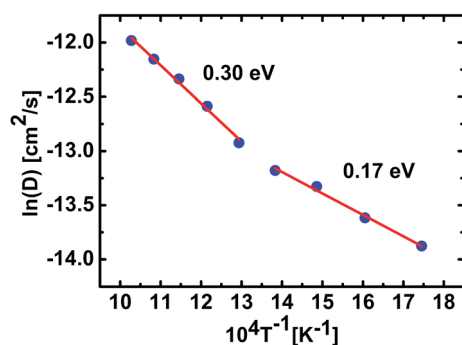


Fig. 5 The average mean square displacement (MSD) for Na, O, and Si ions in amorphous  $\text{Na}_2\text{Si}_2\text{O}_5$  simulated in a temperature range from 573 to 973 K (in steps of 50 K) for 40 ps.



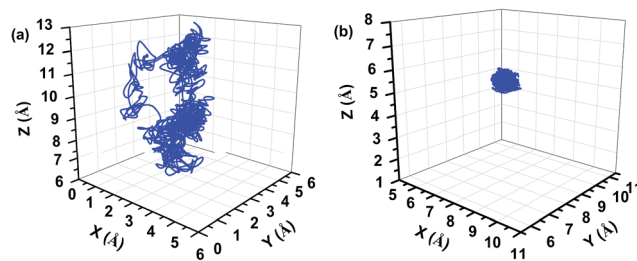
**Table 2** Diffusion coefficient ( $D$  in  $10^{-6} \text{ cm}^2 \text{ s}^{-1}$ ) and conductivity ( $\sigma$  in  $\text{S cm}^{-1}$ ) of  $\text{Na}^+$ 

$T$ (K)	$D_{\text{Na}}$	$D_{\text{O}}$	$D_{\text{Si}}$	$\sigma_{\text{Na}}$	$\sigma_{\text{ex}}$
573	0.94	0.12	0.04	0.051	
623	1.22	0.10	0.05	0.061	
673	1.63	0.03	0.02	0.075	0.005
723	1.89	0.09	0.04	0.081	0.008
773	2.44	0.02	0.02	0.098	0.021
823	3.42	0.05	0.02	0.129	
873	4.39	0.13	0.05	0.156	
923	5.27	0.20	0.13	0.178	
973	6.26	0.07	0.04	0.200	

**Fig. 6** Arrhenius plot of  $\text{Na}^+$  diffusivity in amorphous  $\text{Na}_2\text{Si}_2\text{O}_5$ . A discontinuity at 773 K is observed.

correlations between the hopping movements of mobile ions.<sup>26</sup> It is common to assume that the self-diffusion coefficient  $D$  is equal to the tracer diffusivity  $D^*$  because of the nature that they both describe the ability of an ion to diffuse under no concentration gradient. It was also shown in ref. 27 that the charge diffusivity of  $\text{Na}^+$  was very close to its tracer diffusivity for soda-lime silicate glass. Therefore,  $H_{\text{R}}$  was taken as 1 in the present study.

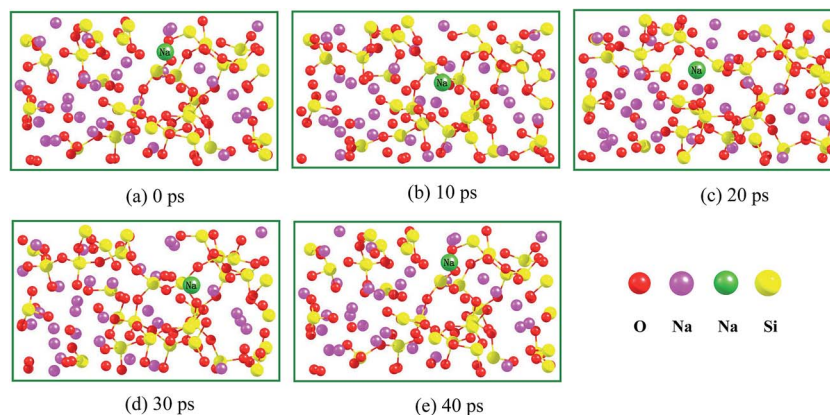
Table 2 summarizes the calculated average  $D$  values of  $\text{Na}^+$ ,  $\text{O}^{2-}$  and  $\text{Si}^{4+}$  at each temperature. Clearly, the  $D$  of  $\text{Na}^+$  is about two orders of magnitude higher than those of  $\text{O}^{2-}$  and  $\text{Si}^{4+}$ , confirming that amorphous  $\text{Na}_2\text{Si}_2\text{O}_5$  is a  $\text{Na}^+$  but not an  $\text{O}^{2-}$  or

**Fig. 8** The calculated ion transport trajectories in amorphous  $\text{Na}_2\text{Si}_2\text{O}_5$ . (a) For  $\text{Na}^+$  and (b)  $\text{O}^{2-}$ . The AIMD was run at 873 K for 40 ps.

$\text{Si}^{4+}$  conductor. Compared to  $\text{Na}^+ \cdot \beta''\text{-Al}_2\text{O}_3$ , a well-known  $\text{Na}^+$ -conductor,  $D_{\text{Na}}$  is roughly one-order of magnitude lower.<sup>28</sup> It is also interesting to note that  $D_{\text{Na}}$  is approximately two-to-three orders of magnitude higher than that of the glass  $\text{Na}_2\text{O} \cdot 2\text{SiO}_2$  at  $T < T_{\text{g}}$ , ( $T_{\text{g}} = 465^\circ \text{C}$  here is the glass transition temperature), whereas it is in good agreement with that of the glass  $\text{Na}_2\text{O} \cdot 2\text{SiO}_2$  at  $T > T_{\text{g}}$ .<sup>29</sup> It is worth mentioning that the low  $D_{\text{O}}$  and  $D_{\text{Si}}$  values are well within the uncertainty of the method considering the limited total run time (40 ps) for the MD simulation and the size of the cell (144 atoms) employed. With a longer MD time and larger cell size, the accuracy of the simulation can be further improved.

The cause for the low  $\text{O}^{2-}$  diffusivity is the strong bonding between O and Si in the stable  $\text{SiO}_4$  tetrahedra, which is consistent with the analysis of partial RDFs. It is also noted that, while  $D_{\text{Na}}$  increases in general with temperature, a peculiar sudden increase is observed at 773 K, implying that a possible phase transition occurred at this temperature. Although the precise reason for the discontinuity is not clear at the present time, 773 K does coincide with the glass-to-ceramic transition temperature identified by DSC and high-temperature XRD.<sup>30</sup>

Table 2 also compares the measured conductivity of amorphous  $\text{Na}_2\text{Si}_2\text{O}_5$  with the simulated one at different temperatures. In general, they are in the same  $10^{-3}$  to  $10^{-2} \text{ S cm}^{-1}$  order of magnitude. Other than the likely small compositional difference between the theoretical  $\text{Na}_2\text{Si}_2\text{O}_5$  and experimental sample that may contain a partial crystalline phase formed during synthesis, the lower experimental  $\sigma$  could also be related to the continuous

**Fig. 7** The  $\text{Na}^+$  transport in amorphous  $\text{Na}_2\text{Si}_2\text{O}_5$  simulated at 873 K for 40 ps. The green ball represents the  $\text{Na}^+$  in motion.

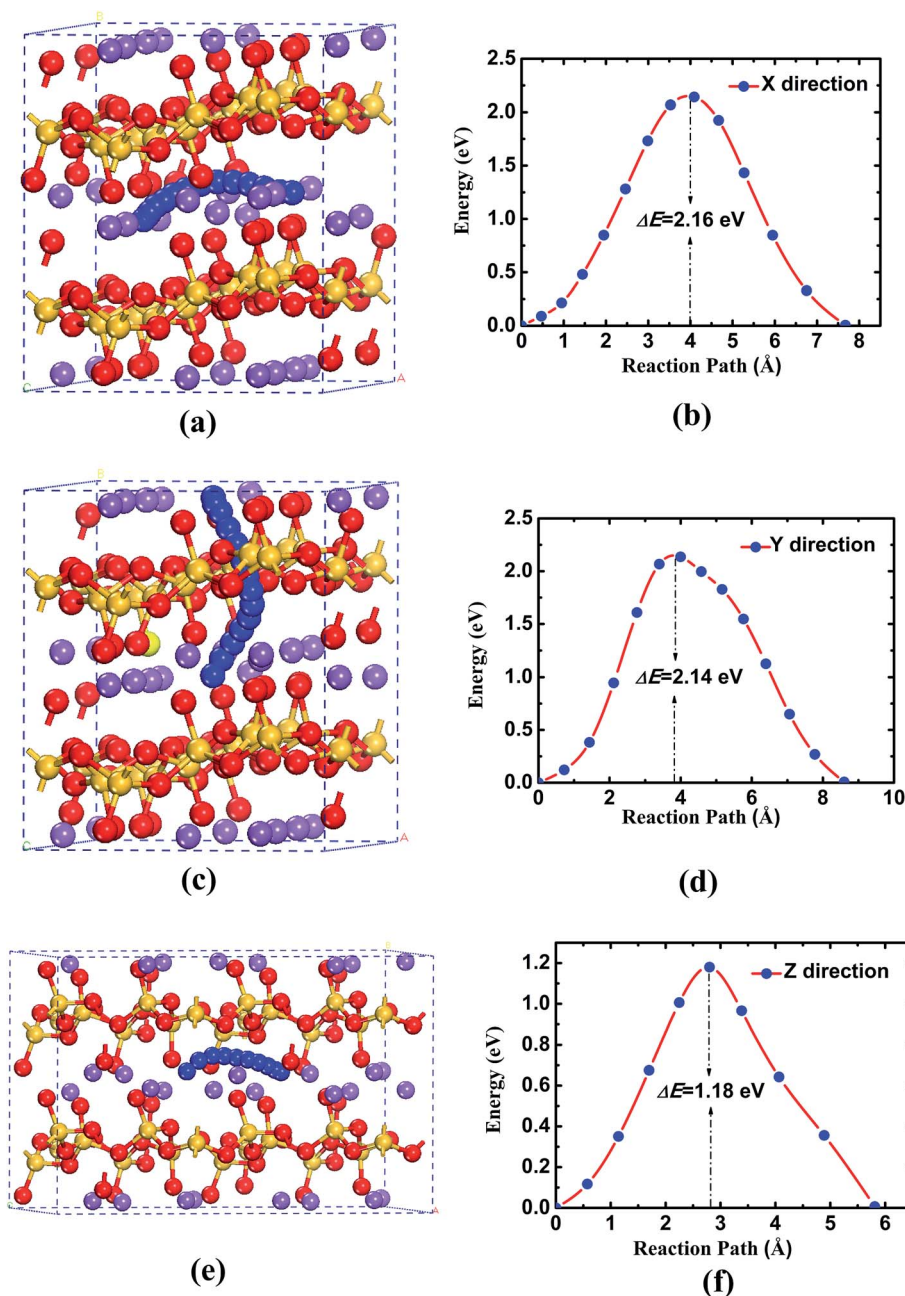


Fig. 9 The minimum energy transport pathways and calculated corresponding energy profiles of a single Na<sup>+</sup> along the X direction (a) and (b), Y direction (c) and (d), and Z direction (e) and (f). The red, golden, and purple balls represent O, Si, and Na ions, respectively. The blue balls are the moving Na<sup>+</sup>. The pathway with the lowest energy is along the Z-direction, which is between two adjacent SiO<sub>4</sub> layers.

crystallization of amorphous Na<sub>2</sub>Si<sub>2</sub>O<sub>5</sub> during the conductivity measurement; the latter has been thoroughly discussed in our recent publication.<sup>30</sup>

Fig. 6 shows the Arrhenius plot of  $D_{\text{Na}}$ ; a kink is clearly visible at 723–773 K. From the slope of the straight-line, the activation energies ( $E_a$ ) are calculated to be 0.17 and 0.30 eV for the 573–723 K and 773–973 K segments, respectively. While these activation energies are somewhat lower than the previously calculated value of 0.56 eV (ref. 14) and experimental result of 0.69 eV for the Na<sub>2</sub>Si<sub>2</sub>O<sub>5</sub> glass,<sup>31</sup> the  $E_a = 0.30$  eV for the 773–973 K segment is in good agreement with 0.222–0.276 eV within 100–370 °C and 0.15–

0.19 eV at >370 °C reported for Na-β''-Al<sub>2</sub>O<sub>3</sub>,<sup>28</sup> but lower than 0.60 eV of a NASICON-type Na<sup>+</sup>-conductor.<sup>32</sup> Moreover, the calculated  $E_a$  is very close to 0.32 eV observed for the Sr<sub>3–3x</sub>Na<sub>3x</sub>Si<sub>3</sub>O<sub>9–1.5x</sub> ( $x = 0.45$ ) (SNS) compound.<sup>7</sup> Compared to other known oxide-ion conductors, viz. 0.53 eV and 0.64 eV for Sr-doped La<sub>10</sub>Si<sub>6</sub>O<sub>27</sub> (ref. 33) and Gd-doped CeO<sub>2</sub> electrolytes, respectively, the calculated  $E_a$  shows a lower value.<sup>34</sup> The corresponding pre-exponential factors for the Na<sup>+</sup> diffusion are  $0.3 \times 10^{-4}$  and  $2.4 \times 10^{-4}$  cm<sup>2</sup> s<sup>−1</sup>, respectively, which is in the same order of magnitude as  $2.6 \times 10^{-4}$  cm<sup>2</sup> s<sup>−1</sup> obtained from the previous MD simulation.<sup>14</sup> The differences observed between this study and a previous one are

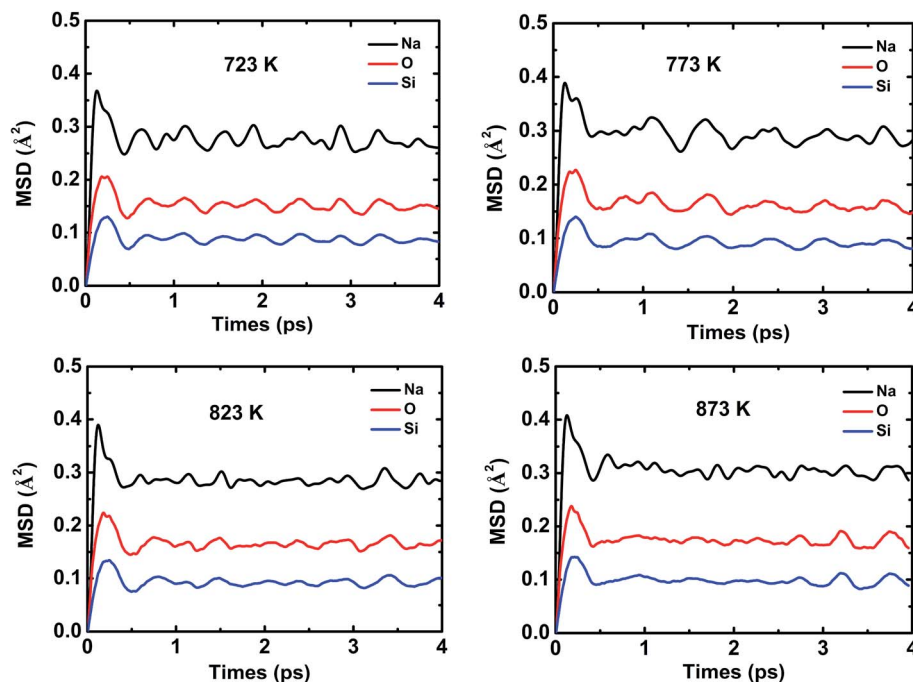


Fig. 10 The averaged MSD for Na, O, and Si ions in the crystalline  $\text{Na}_2\text{Si}_2\text{O}_5$  simulated in a temperature range from 723 to 873 K (in steps of 50 K) for 8 ps.

probably attributed to the different computational method employed and temperature range studied; the latter simulation used the empirical pair-potential method over a temperature range of 1000–2000 K.

**3.1.5 The diffusion pathway of  $\text{Na}^+$ .** The knowledge of  $\text{Na}^+$  diffusion pathways is critically important for the understanding of ionic transport mechanisms in amorphous  $\text{Na}_2\text{Si}_2\text{O}_5$ . Fig. 7(a)–(e) show a series of the snapshots of  $\text{Na}^+$  positions at 873 K in a time interval of 10 ps for a total of 40 ps; the green ball represents one  $\text{Na}^+$  in motion. Comparison of  $\text{Na}^+$  positions at each snapshot indicates a fast  $\text{Na}^+$  diffusion as evidenced by the appreciable positional change of each snapshot. The corresponding trajectory traces of  $\text{Na}^+$  as well as  $\text{O}^{2-}$  are further depicted in Fig. 8. Evidently, the  $\text{Na}^+$  trajectory is 2-dimensional along the  $z$ -axis (or  $c$ -axis in the lattice coordinate, *viz.* parallel to the  $\text{SiO}_4$  layer) with large displacement. In contrast, the simulated  $\text{O}^{2-}$  trajectory is represented by a group of random and unsuccessful jumps with a much smaller displacement.

Another distinct feature of the  $\text{Na}^+$  trajectories is that they are separated into modes associated with the vibration at a fixed site and transport between two sites. This observation provides strong evidence that  $\text{Na}^+$ -transport occurs by discrete hops between two adjacent sites. In other words, Na ions are localized at a particular site for several oscillation periods before jumping to another site at a near distance. A similar hopping mechanism has also been proposed for the same material.<sup>14</sup>

### 3.2. $\text{Na}^+$ transport in the crystalline $\text{Na}_2\text{Si}_2\text{O}_5$

To investigate if the high mobility of  $\text{Na}^+$  is a unique feature of amorphous  $\text{Na}_2\text{Si}_2\text{O}_5$ , we also simulated  $\text{Na}^+$  diffusion dynamics in a crystalline  $\text{Na}_2\text{Si}_2\text{O}_5$ . To do so, one Na atom is virtually

removed from the lattice to create a Na vacancy, followed by  $\text{Na}^+$  hopping *via* Na-vacancies. Based on the symmetry of the  $\text{Na}_2\text{Si}_2\text{O}_5$  crystal structure, three distinct directions, namely,  $X$ ,  $Y$  and  $Z$ , were specified for  $\text{Na}^+$  transport; see Fig. 9(a), (c), and (e). It is worth mentioning that along the  $Z$ -direction  $\text{Na}^+$  is transported between the two corner-shared  $\text{SiO}_4$  layers. The corresponding energy profiles optimized for  $\text{Na}^+$  transport are shown in Fig. 9(b), (d), and (f). Along the  $X$ -direction, Fig. 9(a) and (b), one can see that the movement of  $\text{Na}^+$  between the two nearest neighbors features an arced pathway with an energy barrier of 2.16 eV. Such a high energy barrier suggests that  $\text{Na}^+$  transportation along the  $X$ -direction is unlikely. Along the  $Y$ -direction, Fig. 9(c) and (d), the path between the two nearest neighbors is longer and features a zigzag pathway passing through the  $\text{SiO}_4$  tetrahedral layers. The energy barrier is as high as 2.14 eV, indicating that  $\text{Na}^+$  movement along the  $Y$ -direction is also less favorable. The lowest energy barrier is 1.18 eV observed for the movement along the  $Z$ -direction, Fig. 9(e) and (f), a two-dimensional channel formed by corner-shared  $\text{SiO}_4$  tetrahedra, although it is probably too high for a fast  $\text{Na}^+$  transport.

To further confirm that fast  $\text{Na}^+$  conduction is unique for amorphous  $\text{Na}_2\text{Si}_2\text{O}_5$ , we also performed *ab initio* molecular dynamics simulations on crystalline  $\text{Na}_2\text{Si}_2\text{O}_5$  at 723, 773, 823, and 873 K, respectively, for 8 ps. The parameters of AIMD were the same as those used in amorphous  $\text{Na}_2\text{Si}_2\text{O}_5$ . The mean square displacements (MSDs) for Na, O, and Si ions simulated at these temperatures are shown in Fig. 10. It is evident that the MSDs indicate no significant  $\text{Na}^+$  diffusion in the crystalline  $\text{Na}_2\text{Si}_2\text{O}_5$  as in the amorphous counterpart at elevated temperatures.

Overall, it is rather clear that  $\text{Na}^+$  transport in amorphous  $\text{Na}_2\text{Si}_2\text{O}_5$  is much faster than that in the crystalline form. One



fundamental reason is that the high energy barrier for  $\text{Na}^+$  through channels formed by corner-shared  $\text{SiO}_4$  tetrahedra in the crystalline  $\text{Na}_2\text{Si}_2\text{O}_5$  is significantly lowered by the long-range disordering in amorphous phase  $\text{Na}_2\text{Si}_2\text{O}_5$ , thus increasing  $\text{Na}^+$  conductivity.

## IV. Conclusions

The AIMD simulations of ionic transport in amorphous  $\text{Na}_2\text{Si}_2\text{O}_5$  strongly suggest that the predominant mobile charge carrier is  $\text{Na}^+$ . The MSD of  $\text{Na}^+$  features a linear increase with time whereas those of  $\text{O}^{2-}$  and  $\text{Si}^{4+}$  show time-independent plateaus. The RDF analysis further reveals the absence of Na–Na separation in the total  $g(r)$ , implying a fast  $\text{Na}^+$  conduction. The movement of  $\text{Na}^+$  in amorphous  $\text{Na}_2\text{Si}_2\text{O}_5$  is a low-energy process, yielding a self-diffusivity at least two orders of magnitude higher than that of  $\text{O}^{2-}$  and  $\text{Si}^{4+}$ . The simulated activation energy for  $\text{Na}^+$  agrees well with those reported in the literature for the well-known  $\text{Na}^+$ -conductor  $\text{Na}-\beta''\text{-Al}_2\text{O}_3$ . The calculated conductivity is found to be higher than the experimental data, the reason for which is related to the continuous glass-to-ceramic transition experienced during the experimental conductivity measurement, resulting in lowered conductivity. The simulation of  $\text{Na}^+$  transport pathways indicates that  $\text{Na}^+$  preferentially diffuses within the layered channels formed by corner-shared  $\text{SiO}_4$  tetrahedra in short-range ordering and long-range disordering. A similar simulation of  $\text{Na}^+$  across a crystalline  $\text{Na}_2\text{Si}_2\text{O}_5$  suggests that crystalline  $\text{Na}_2\text{Si}_2\text{O}_5$  is virtually an electrical insulator with a high energy barrier. Among the three crystallographic directions simulated, the energy barrier is the lowest for the  $Z$ -direction, along the layers formed by corner-shared  $\text{SiO}_4$  tetrahedra. Overall, amorphous  $\text{Na}_2\text{Si}_2\text{O}_5$  is a promising  $\text{Na}^+$  conductor.

## Acknowledgements

This work was funded by the Advanced Research Projects Agency-Energy (ARPA-E), U.S. Department of Energy, under Award number DE-AR0000492. Partial support from NSF (CBET-1264706) is also acknowledged. We would also like to thank the National Energy Research Scientific Computing Center (NERSC) of US Department of Energy for awarding us computational hours to complete the molecular dynamics calculations.

## References

- 1 A. J. Jacobson, *Chem. Mater.*, 2010, **22**, 660.
- 2 L. Malavasi, C. A. J. Fisher and M. S. Islam, *Chem. Soc. Rev.*, 2010, **39**, 4370.
- 3 A. Aguadero, L. Fawcett, S. Taub, R. Woolley, K. Wu, N. Xu, J. A. Kilner and S. J. Skinner, *J. Mater. Sci.*, 2012, **47**, 3925.
- 4 P. Singh and J. B. Goodenough, *Energy Environ. Sci.*, 2012, **5**, 9626–9631.
- 5 P. Singh and J. B. Goodenough, *J. Am. Chem. Soc.*, 2013, **135**, 10149–10154.
- 6 R. Martinez, P. Singh, J. A. Alonso and J. B. Goodenough, *J. Mater. Chem. A*, 2014, **2**, 4355–4360.
- 7 T. Wei, P. Singh, Y. Gong, J. B. Goodenough, Y. Huang and K. Huang, *Energy Environ. Sci.*, 2014, **7**, 1680–1684.
- 8 J. G. Xu, X. M. Wang, H. Fu, C. M. Brown, X. P. Jing, F. H. Liao, F. Q. Lu, X. H. Li, X. J. Kuang and M. M. Wu, *Inorg. Chem.*, 2014, **53**, 6962.
- 9 R. D. Bayliss, S. N. Cook, S. Fearn, J. A. Kilner, C. Greaves and S. J. Skinner, *Energy Environ. Sci.*, 2014, **7**, 2999.
- 10 R. D. Bayliss, S. N. Cook, D. O. Scanlon, S. Fearn, J. Cabana, C. Greaves, J. A. Kilner and S. J. Skinner, *J. Mater. Chem. A*, 2014, **2**, 17919.
- 11 I. R. Evans, J. S. O. Evan, H. G. Davies, A. R. Haworth and M. L. Tate, *Chem. Mater.*, 2014, **26**, 5187.
- 12 C. Tealdi, L. Malavasi, I. Uda, C. Ferrara, V. Berbenni and P. Mustarelli, *Chem. Commun.*, 2014, **50**, 14732.
- 13 S. Fernández-Palacios, L. Santos-Gómez, J. M. Compañ, J. M. Porras-Vázquez, A. Cabeza, D. Marrero-López and E. R. Losilla, *Ceram. Int.*, 2015, **41**, 6542.
- 14 W. Smith, G. N. Greaves and M. J. Gillan, *J. Chem. Phys.*, 1995, **103**(8), 22.
- 15 W. Smith, G. N. Greaves and M. J. Gillan, *J. Non-Cryst. Solids*, 1995, **192–193**, 267–271.
- 16 W. Smith, T. R. Forester, G. N. Greaves, S. Haytera and M. J. Gillan, *J. Mater. Chem.*, 1997, **7**(2), 331–336.
- 17 P. E. Blöchl, Projector augmented-wave method, *Phys. Rev. B: Condens. Matter Mater. Phys.*, 1994, **50**, 17953–17979.
- 18 G. Kresse and D. Joubert, From ultrasoft pseudopotentials to the projector augmented-wave method, *Phys. Rev. B: Condens. Matter Mater. Phys.*, 1999, **59**, 1758–1775.
- 19 G. Kresse and J. Hafner, *Phys. Rev. B: Condens. Matter Mater. Phys.*, 1993, **47**, RC558–561.
- 20 G. Kresse and J. Furthmüller, *Phys. Rev. B: Condens. Matter Mater. Phys.*, 1996, **54**, 11169–11186.
- 21 J. P. Perdew, K. Burke and M. Ernzerhof, Generalized gradient approximation made simple, *Phys. Rev. Lett.*, 1996, **77**, 3865–3868.
- 22 G. Mills and H. Jónsson, *Phys. Rev. Lett.*, 1994, **72**, 1124–1127.
- 23 G. Mills, H. Jónsson and G. K. Schenter, *Surf. Sci.*, 1995, **324**, 305–337.
- 24 M. E. Fleet and G. S. Henderson, *J. Solid State Chem.*, 1995, **119**, 400–404.
- 25 M. Misawa, D. L. Price and K. Suzuki, *J. Non-Cryst. Solids*, 1980, **37**, 85–97.
- 26 G. E. March, *Solid State Ionics*, 1982, **7**, 177–198.
- 27 H. Mehrer, A. W. Imre and E. Tanguen-Nijokep, *J. Phys.: Condens. Matter*, 2008, **106**, 012001.
- 28 F. Tietz and W. Umland, *Solid State Ionics*, 1995, **78**, 35.
- 29 Ch. Kaps, *J. Non-Cryst. Solids*, 1984, **65**, 189–192.
- 30 Y. Jee, X. Zhao and K. Huang, *Chem. Commun.*, 2015, **51**, 9640–9642.
- 31 G. H. Frischat, *Ionic Diffusion in Oxide Glasses*, Trans. Tech., Aedermannsdorf, 1975.
- 32 C. Verissimo, F. M. S. Garridol, O. L. Alves, P. Calle, A. Martínez-Juárez, J. E. Iglesia and J. M. Rojo, *Solid State Ionics*, 1997, **100**, 127.
- 33 H. Arikawa, H. Nishiguchi, T. Ishihara and Y. Takita, *Solid State Ionics*, 2000, **136–137**, 31–37.
- 34 B. C. H. Steele, *Solid State Ionics*, 2000, **129**, 95–110.